Title

Age Associated Increase in Microglia Inflammation and Phagocytosis in the Adult Neural Stem Cell Niche

Authors

Ronald Cutler[1, =], Samuel Harrison[1, =], Natalia Sandoval-Kuhn[1], Stephen Tomlinson[2], Erzsebet Kokovay[1, *]

Affiliations

[1] UTH-SA, Department of Cell Systems and Anatomy, San Antonio, TX, USA

[2] Medical University of South Carolina, Department of Pharmacology and Immunology, Charleston, SC, USA

[=] Authors contributed equally to this work

[*] Correspondence to E.K. (KokovayE@uthscsa.edu)

Abstract

Adult SVZ neurogenesis declines with age, but the niche mechanisms remain incompletely defined. Here, we show that SVZ microglia acquire activation-associated morphology with aging. Reanalysis of published SVZ single-cell RNA-Seq data revealed that aged microglia upregulate inflammatory and lysosome/phagosome-related gene programs, including multiple phagocytosis-associated receptors and effectors. Functionally, young SVZ-derived microglia exhibit reduced basal phagocytic activity compared with non-SVZ microglia *in vitro*, whereas aged SVZ microglia show increased phagocytosis. *In vivo* SVZ wholemounts reveal increased progenitor-derived material within lysosomal compartments of microglia with age, without an accompanying increase in SVZ apoptosis. Inhibiting complement C3 activation or reducing inflammation with minocycline treatment partially restores SVZ proliferation in aged mice, but does not reduce progenitor-derived material within lysosomal compartments of aged microglia. These data support a model in which microglial inflammatory signaling contributes to age-related suppression of SVZ proliferation, while microglial engagement with neural progenitors is sustained by additional mechanisms.

Introduction

Adult neural stem cells (NSCs) reside in two principal neurogenic niches of the rodent brain: the subgranular zone (SGZ) of the dentate gyrus and the subventricular zone (SVZ) lining the lateral ventricles. In the current study, we are focused on the NSCs in the SVZ niche, which exist in quiescent (qNSCs) and activated (aNSCs) states and generate transit amplifying cells (TACs), that expand and then produce migratory neuroblasts (Alvarez-Buylla & García-Verdugo, 2002; Doetsch et al., 1999; Lim & Alvarez-Buylla, 2016). These neuroblasts migrate from the SVZ through the RMS into the OB where they differentiate and integrate into local circuitry (Alvarez-Buylla & García-Verdugo, 2002). With aging, multiple studies report reduced SVZ neurogenesis accompanied by decreased NSC proliferation, increased NSC quiescence, and diminished NSC pool size (Ahlenius et al., 2025; Cutler & Kokovay, 2020; Enwere et al., 2004; Kalamakis et al., 2019; Maslov et al., 2004; Solano et al., 2016). These findings motivate work aimed at identifying niche-derived mechanisms that constrain activation and lineage progression in the aged SVZ.

Microglia are brain-resident macrophage-lineage cells that survey the parenchyma and shape neural homeostasis through debris clearance, phagocytosis, synapse remodeling, and secretion of signaling factors (Deczkowska et al., 2018). Fate-mapping indicates that microglia originate from early embryonic yolk sac–derived myeloid progenitors that seed the central nervous system and largely self-maintain thereafter (Ginhoux et al., 2010). Microglia constitute a substantial fraction of brain cells (commonly estimated at ~5–15% depending on region and quantification) and display pronounced context-dependent states across development, aging, and disease (Deczkowska et al., 2018).

Several studies suggest that microglia within the SVZ are not interchangeable with microglia in non-neurogenic parenchyma. SVZ-associated microglia exhibit distinct morphological and antigenic features and have been implicated in regulating neurogenesis and progenitor dynamics (Goings et al., 2006; Marshall et al., 2014; Shigemoto-Mogami et al., 2014; Solano et al., 2016; Xavier et al., 2015). Aging is accompanied by microglial state changes in the SVZ, including increased inflammatory and lysosomal programs that precedes the decline of NSC proliferation, raising the possibility that altered microglia–NSC interactions contribute to reduced neurogenesis in the aged SVZ (Solano et al., 2016). Intriguingly, these age-related shifts in microglia towards an activated state are reminiscent of their phenotype in the developing cerebral cortex and SVZ where they have been shown to phagocytose neural precursor cells (Cunningham et al., 2013; Morrison et al., 2023). Furthermore, in a model of cortical ischemic stroke, microglia were reported to phagocytose dying neuroblasts, constraining the endogenous neurogenic response after injury (Nath et al., 2024). Despite evidence that niche inflammation can constrain activation and lineage output, it remains unclear whether aging-associated microglial activation in the SVZ is coupled to changes in microglial phagocytic behavior toward specific NSC populations, and whether inflammatory signaling and phagocytic engagement represent linked or separable mechanisms.

In this study, we test the hypothesis that aging alters SVZ microglial state and microglia–NSC interactions in ways that contribute to diminished progenitor proliferation. We found that during aging, SVZ microglia are characterized by increases in a lysosomal marker and enlarged morphologies, alongside upregulation of pro-inflammatory and phagocytic gene expression signatures, consistent with an pro-phagocytic phenotype. Aged SVZ microglia show increased phagocytosis *in vitro* and *in vivo*, where we found evidence for the engulfment of aNSCs/TACs.

Finally, interventions that reduced inflammation partially restored proliferative measures, but did not reduce aNSC/TAC engulfment, suggesting that microglial inflammatory signaling contributes to reduced NSC proliferation during aging, whereas progenitor phagocytosis is likely regulated by additional mechanisms.

Results

Age-related changes in SVZ microglia morphology

We previously reported that murine SVZ neurogenesis is reduced by 12 months of age (Solano et al., 2016). To assess how SVZ microglia change during aging, we performed immunohistochemistry on SVZ wholemount preparations (to preserve 3D niche cytoarchitecture) from young (3 month) and aged (12 month) mice, staining for the microglial marker Iba1 and the lysosomal marker CD68. In young mice, Iba1+ microglia exhibited a ramified morphology throughout the SVZ with relatively low CD68 signal within Iba1+ cells (Fig. 1A-B). In aged mice, Iba1+ microglia displayed morphology consistent with activation, including fewer processes and enlarged somata, together with increased CD68 signal within Iba1+ cells (Fig. 1C-D). Because microglia can adopt a lysosome-rich, phagocytic phenotype during neuronal development that is associated with engulfment of neural precursor cells, we hypothesized that age-associated microglial activation in the SVZ is accompanied by increased phagocytic activity toward SVZ progenitors (Cunningham et al., 2013).

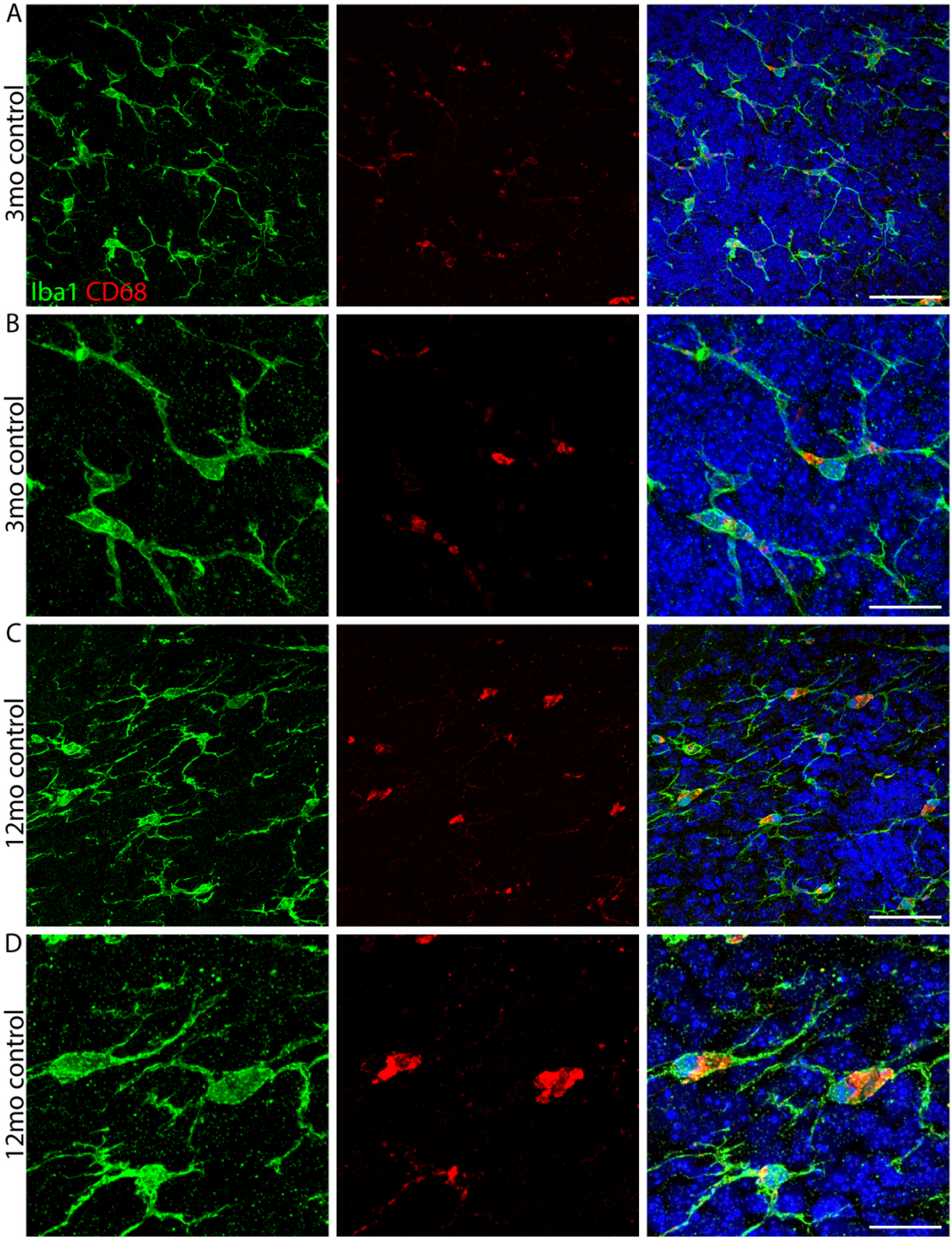
A
3mo control
Iba1 CD68
B
3mo control
C
12mo control
D
12mo control

108

Figure 1. Age-Associated SVZ Microglia Morphological Changes and Increased Activation. Representative confocal projection images of SVZ microglia stained with Iba1 (green), lysosomes stained with CD68 (red), and nuclei stained with DAPI (blue). **(A-B)** Young (3 month) SVZ microglia imaged at 40X magnification (A) or 100X magnification (B). **(C-D)** Aged (12 month) SVZ microglia imaged at 40X magnification (C) or 100X magnification (D). Scale bars in (A) and (C) = 20µm, scale bars in (B) and (D) = 50µm

Gene expression in the aging SVZ suggests increased microglial phagocytic programs

To assess age-related transcriptional changes in SVZ microglia and NSC populations relevant to inflammation and phagocytosis, we reanalyzed a published single-cell RNA-Seq dataset comprising of 14,685 cells from the SVZ of young (3 month) and old (28/29 month) male mice (Dulken et al., 2019). We generated pseudobulk profiles for each cell type and biological replicate, performed differential gene expression analysis (old vs. young), followed with gene set enrichment analysis (GSEA) (Supplementary Figs. 1A-B).

In microglia, we identified 254 genes significantly upregulated and 54 genes significantly downregulated with age (adjusted p-value < 0.05; Supplementary Fig. 1C; Supplementary Table 1). GSEA of genes upregulated with aging revealed enrichment of processes related to translation, secretion of inflammatory cytokines, and lipid metabolism, consistent with prior analyses (Dulken et al., 2019; Yen & Yu, 2024). In contrast, downregulated genes were enriched for cytoskeleton organization terms, which has not been previously reported and may suggest dysfunction in motility or morphology-related programs (Supplementary Fig. 1D).

Although canonical "phagocytosis" terms were not significantly enriched by GSEA (Supplementary Fig. 1D), several phagocytosis-associated receptors, including *Axl* and *Tlr2*, were among the most strongly upregulated transcripts with age (Supplementary Fig. 1C). We therefore curated comprehensive gene sets representing multiple components of phagocytosis from MSigDB (Liberzon et al., 2024) and intersected these with age-related differentially expressed genes (ARDEGs; adjusted p-value < 0.05; Supplementary Table 2). 19 phagocytosis-related genes overlapped with the microglia ARDEG set, of which 18 were upregulated in aged microglia (Fig. 2A; Supplementary Table 3). Notably, 8 of these genes (*Cyba, Atp6v0e, Rab7b, Cybb, Vim, B2m,*

138 *Tlr2,* and *Hvcn1*) are linked to phagosome formation/maturation and vesicular acidification. We
139 further expanded our phagocytosis gene list to include genes identified in prior functional screens
140 (Haney et al., 2018; Pluvinage et al., 2019), and found that all intersecting genes (9/9) were
141 upregulated in aged microglia (Supplementary Figs. 2A-B). Finally, we found that the broad
142 upregulation of phagocytosis-related gene expression was also accompanied by an increase in the
143 expression of genes related to microglia activation (Supplementary Figs. 2C-D). While these
144 transcriptional shifts are consistent with increased lysosomal/phagocytic programs, we note that
145 elevated expression of such genes could also reflect compensatory responses to altered phagocytic
146 demand or efficiency rather than a direct readout of increased engulfment per se. For instance, the
147 expression of the receptor essential for microglial function, *Csf1r*, was downregulated in aged
148 microglia while the ligand *Csf1* showed the opposite trend and thus may be a compensatory
149 response to chronic microglia activation (Supplementary Fig. 2C) (Hu et al., 2024). Together, these
150 findings suggest that aging is accompanied by transcriptional reprogramming of SVZ microglia
151 toward states featuring inflammatory signaling and lysosome/phagosome-related programs, with
152 partial resemblance to developmental and phagocytic microglial states (Cunningham et al., 2013;
153 Izgi et al., 2022).

154 We next asked whether age-associated changes were concentrated within particular receptor-
155 mediated phagocytosis pathways. Using a curated list for the major phagocytosis pathways, we
156 observed upregulation of the receptors in the Complement, TAM, and Toll-like pathways (Fig. 2E;
157 Supplementary Table 3). In contrast, for the FC gamma, Scavenger, P2ry6, and Trem2 receptor
158 pathways, multiple pathway components were consistently upregulated without a corresponding
159 increase in the core receptor transcript (Deczkowska et al., 2018). Notably, while Trem2 itself was
160 not increased, aged microglia displayed expression patterns consistent with a disease-associated

161 microglia (DAM) stage 2 signature that has been reported to be Trem2-dependent in other contexts
162 (Supplementary Fig. 2E). Overall, these results indicate broad multi-pathway upregulation of
163 phagocytosis-related gene expression during aging and suggest that aged SVZ microglia may
164 adopt a unique Trem2-independent DAM-like state.

165 We then analyzed NSC populations for age-associated expression changes in signals relevant to
166 target-cell recognition and engulfment, including apoptosis, "find-me," "eat-me," and "don't eat-
167 me" programs. Compared to microglia, there were very few ARDEGs: 13 genes were significantly
168 upregulated in aged astrocyte-qNSC as compared to young (adjusted p-value < 0.05), whereas no
169 genes met this threshold for aged aNSC, TACs or neuroblasts (Supplementary Figs. 1E-J). Given
170 this limited power for threshold-based overlap analyses, we used GSEA with curated gene sets for
171 apoptosis and phagocytosis-related signaling (Supplementary Table 2).

172 Using this approach, we detected age-associated upregulation of an apoptosis gene set in astrocyte-
173 qNSC cells (adjusted p-value < 0.05), whereas aNSC, TACs and neuroblasts showed the opposite
174 trend (Fig. 2C; Supplementary Fig. 3A). We did not detect significant enrichment for curated "find-
175 me" or generic "eat-me" gene sets. However, we observed age-associated upregulation of
176 complement system and opsonization gene sets (often considered "eat-me"–adjacent signals) in
177 astrocyte-qNSCs and neuroblasts, but not in aNSCs or TACs (Fig. 2C; Supplementary Fig. 3B,C)
178 (Li, 2012). Intriguingly, astrocyte-qNSCs and neuroblasts also showed increased expression of a
179 curated "don't eat-me" gene set (Fig. 2C; Supplementary Fig. 3D). This set includes genes related
180 to MHC class I antigen presentation such as *H2-K1* and *H2-D1*, which in some contexts can oppose
181 macrophage phagocytosis, particularly when expressed with *B2m* (Supplementary Fig. 3D)
182 (Khalaji et al., 2023). Consistent with a potential receptor–ligand axis, *Lilrb4a*, an inhibitory
183 receptor for MHC class I, was among the age-upregulated microglial ARDEGs (Supplementary

184 Fig. 1C). An antigen processing/presentation gene set showed a similar pattern to the "don't eat-
185 me" set, further supporting increased MHC class I–associated programs in aged astrocyte-qNSCs
186 and neuroblasts, but not aNSC-NPCs (Supplementary Fig. 1E).

187 In summary, transcriptomic changes in SVZ microglia with age are consistent with increased
188 inflammatory and lysosome/phagosome-related programs across multiple receptor pathways. In
189 aged NSC populations, astrocyte-qNSCs and neuroblasts showed increased complement pathway
190 components ("eat-me" signals) together with increased expression of putative "don't eat-me" anti-
191 phagocytic signals, while aNSC-NPCs did not show comparable upregulation of those signals.
192 These patterns are consistent with a model in which age-associated microglial phagocytic
193 programs may preferentially engage aNSC/TACs.

194

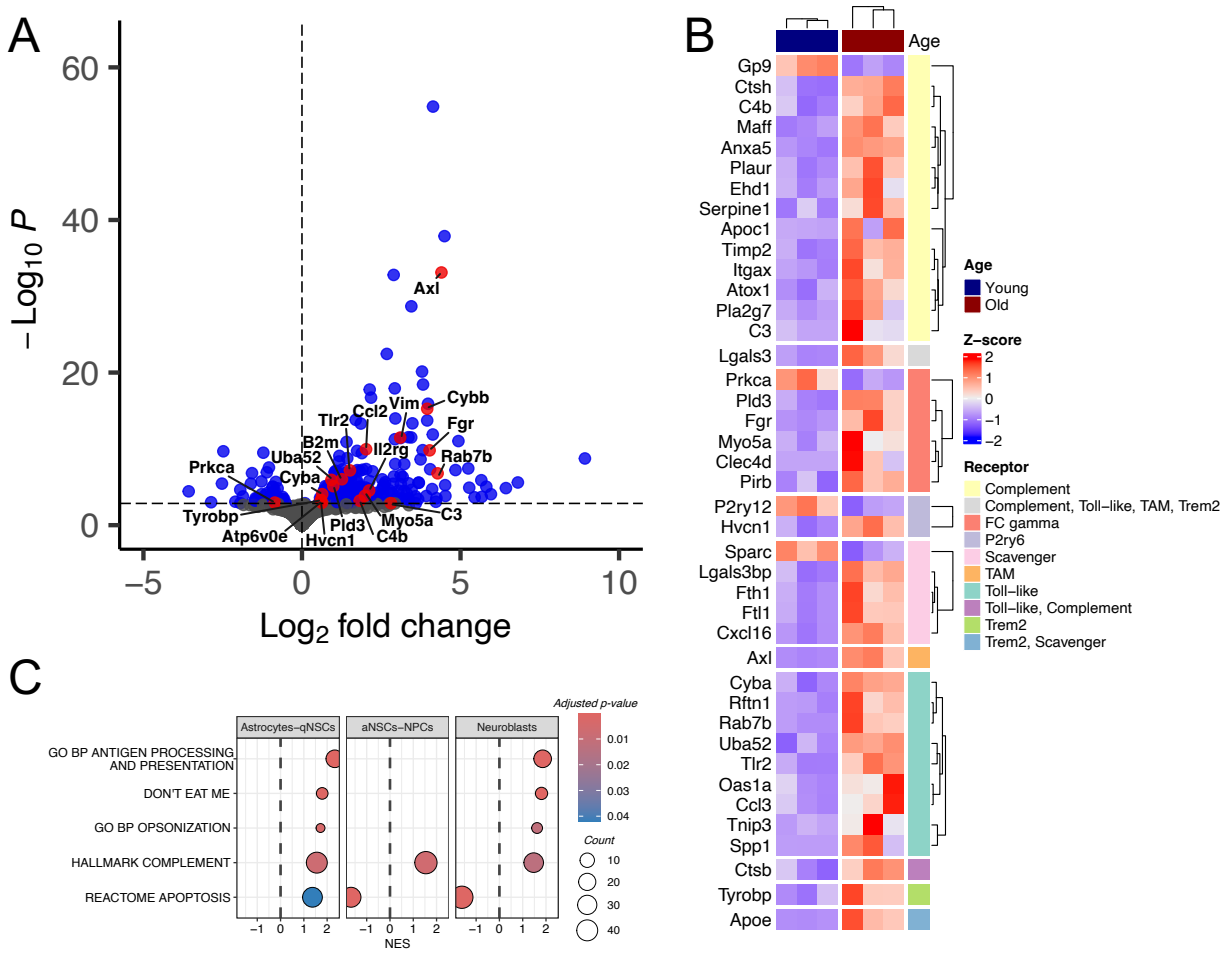

Figure 2. Gene expression in the aging SVZ suggests increased microglial phagocytic programs

(A) Pseudobulk level analysis of differential gene expression changes during aging of young (3 month) and aged (28–29 month) microglia in the SVZ. Red points indicate genes that overlapped with the phagocytosis-related gene sets (Supplementary table 2) which have absolute log2 fold change > 1 and adjusted p-value < 0.05. Statistics: n=3 mice/group, DGE results obtained using Wald test followed by Benjamini-Hochberg correction for multiple hypothesis testing. **(B)** Heatmap of age-related DEGs (adjusted p-value < 0.05) in aging SVZ microglia (obtained from analysis in (A)) that overlapped with phagocytosis-related gene sets (Supplementary table 2) Statistics: n=3 mice/group. **(C)** Gene set enrichment analysis of age-related gene expression changes in neural progenitor cells using apoptosis, "find-me," "eat-me," and "don't eat-me" signal gene sets (Supplementary table 2). Statistics: n=3 mice/group, GSEA p-values obtained using a permutation test followed by followed by Benjamini-Hochberg correction for multiple hypothesis testing.

212 **SVZ microglia show an age-associated increase in phagocytic activity toward**
213 **SVZ progenitors**

214 To assess SVZ microglia phagocytic activity, we microdissected the SVZ and isolated microglia
215 either from the SVZ or from the remainder of the brain (excluding the SVZ) from young (3 month)
216 and aged (12 month) mice. Isolated microglia were expanded *in vitro*, and phagocytosis was
217 quantified by live imaging of engulfment of pHrodo-conjugated yeast particles (pH-sensitive
218 reporter that fluoresces upon acidification in phagolysosomes) (Kapellos et al., 2016). In young
219 animals, SVZ-derived microglia displayed lower phagocytic activity than microglia isolated from
220 non-SVZ brain regions under our assay conditions, consistent with niche-associated specialization
221 toward reduced basal phagocytosis (Fig. 3A) (Xavier et al., 2015). In aged animals, SVZ-derived
222 microglia showed a significant increase in phagocytic activity relative to young SVZ microglia,
223 approaching the levels observed in whole-brain microglia.

224 We next sought *in vivo* evidence that the age-associated increase in SVZ microglial phenotypes
225 reflects increased phagocytic engagement with SVZ progenitors. As an initial test, we quantified
226 apoptosis in the SVZ by immunohistochemistry for cleaved caspase-3 on coronal sections from
227 young (3 month) and aged (12 month) mice and did not detect a significant age-associated increase
228 in apoptotic cells in the SVZ (Fig. 3B). Next, we sought to validate the findings of an age-related
229 increase in SVZ microglia phagocytosis activity in our *in vitro* system by examining SVZ
230 microglia phagocytosis *in vivo*. We assessed microglial phagolysosomal content directly by
231 staining SVZ wholemounts for Iba1 (microglia), CD68 (lysosomes), and Mash1 (aNSC/TAC
232 specific transcription factor) (Kim et al., 2011; Lim & Alvarez-Buylla, 2016). In both young and
233 aged SVZ, we observed Mash1 signal within CD68+ compartments inside Iba1+ microglia (Fig.

234 3D). Quantification indicated that ~20% of SVZ microglia contained Mash1+ material within
235 CD68+ compartments in young mice, and this fraction increased over 2-fold at 12 months of age
236 (Fig. 3C). Together, these in vitro and in vivo data support an age-associated increase in SVZ
237 microglial phagocytic activity and increased microglial phagolysosomal association with
238 progenitor-derived material in the aged SVZ.

239

240

241

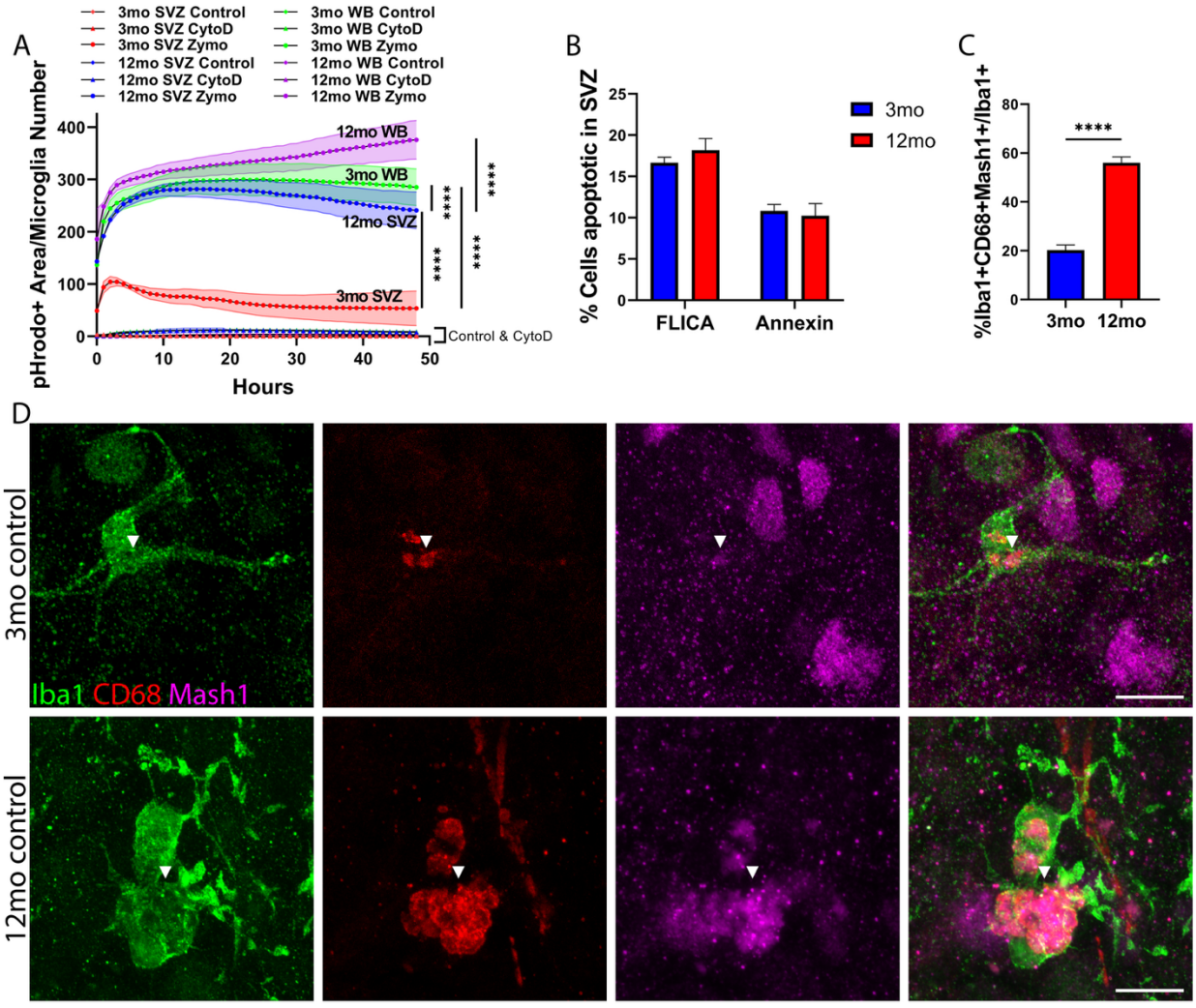

Figure 3. SVZ microglia show an age-associated increase in phagocytic activity toward SVZ progenitors. (A) Time-lapse *in vitro* phagocytosis assay of young (3 months) or aged (12 months) SVZ or whole brain (WB) microglia labeled with isolectin and incubated with Zymosan-pHrodo (Zymo), CytochalasinD and Zymosan-pHrodo (CytoD, negative control), or isolectin only (Control). Phagocytosis is quantified as pHrodo+ area indicated by red fluorescence / microglia number. Statistics: n=3 mice/group, ≥ 1,000 microglia quantified per mouse. (B) Quantification of Caspase 3 in SVZ whole mounts. Statistics: n=6 mice/group, p-value estimated using two-way ANOVA. (C) Quantification of *in vivo* phagocytosis of 3- or 12-month SVZ microglia measured as Iba1+CD68+Mash1+ microglia / total Iba1+ microglia (Methods). *n*=11 mice/group, ≥100 microglia quantified per mouse. (D) Representative confocal projection images of young or aged SVZ microglia stained with Iba1 (green), microglia lysosomes stained with CD68 (red), and TAC transcription factor stained with Mash1 (magenta). Scale bar: 10µm, p-value estimated using two-way ANOVA. P-value legend: ns: no symbol; ****: $p \leq 0.0001$.

257 **Complement inhibition partially rescues SVZ proliferation in aged mice yet**
258 **further increases SVZ microglia phagocytosis**

259 To explore possible mechanisms that might contribute to the age-associated increase in SVZ
260 microglial phagocytic engagement of aNSC/TAC populations in the SVZ, we examined expression
261 of candidate pro-inflammatory factors in SVZ microglia guided by our transcriptomic reanalysis
262 (Fig. 2A). We reasoned that pro-inflammatory genes that were low or absent in the young SVZ
263 microglia relative to non-SVZ microglia that are increased with age in SVZ microglia would be
264 good candidates based on our *in vitro* phagocytosis results (Fig. 3A). Among the candidates, *C3*
265 (Complement component 3) showed higher expression in non-SVZ microglia relative to young
266 SVZ microglia and was strongly upregulated with age in SVZ microglia (Supplementary Fig. 4).
267 In addition, transcripts encoding *C3* receptors *Itgam* and *Itgax* were increased in aged SVZ
268 microglia. Based on these observations, we tested whether inhibiting *C3* activation would alter
269 SVZ proliferation and/or microglial phagocytic readouts *in vivo*.

270 To inhibit C3 cleavage and deposition, we used CR2-Crry, a targeted complement inhibitor that
271 crosses the blood brain barrier and localizes to sites of complement activation via CR2 to then
272 block C3 activation through Crry (Atkinson et al., 2005; Song et al., 2003). Young (3 month) and
273 aged (12 month) mice received CR2-Crry or saline every other day for three total doses, followed
274 by a 2-hour EdU pulse prior to sacrifice to label proliferating cells (Fig. 4A). SVZ wholemounts
275 were collected and processed for immunohistochemistry as described above (Methods).

276 In young mice, CR2-Crry treatment did not significantly affect SVZ proliferation as indicated by
277 EdU+ cells, microglial CD68 area, or the fraction of microglia containing Mash1+ material within
278 CD68+ compartments (Fig. 4B-G). As expected, saline-treated aged mice showed reduced SVZ

279 proliferation relative to saline-treated young mice (Fig. 4F). In aged mice, CR2-Crry significantly
280 increased SVZ proliferation compared with age-matched saline controls as indicated by EdU+
281 cells (Fig. 4F). CD68 area per Iba1+ microglia was increased in aged saline-treated mice relative
282 to young controls (Fig. 4B), however, CR2-Crry produced a non-significant reduction in this
283 measure in aged mice (Fig. 4B). Notably, the microglia containing Mash1+ material within CD68+
284 compartments increased with age, but were not reduced by CR2-Crry treatment; instead, this was
285 increased in aged CR2-Crry–treated mice relative to aged saline controls (Fig. 4G).

286 Together, these data indicate that complement inhibition via CR2-Crry can partially restore
287 proliferative output in the aged SVZ, but does not decrease, under these conditions and readouts,
288 microglial lysosomal association with Mash1+ progenitor material. One interpretation is that
289 complement-dependent inflammation contributes to reduced SVZ proliferation, whereas the
290 phagocytic engagement captured by the CD68/Mash1 colocalization assay is regulated by
291 additional mechanisms. An alternative, non-mutually exclusive explanation is that increasing
292 progenitor production in aged mice increases the availability of Mash1+ material, thereby
293 maintaining or elevating the colocalization readout even if per-cell phagocytic engagement were
294 unchanged. Distinguishing these possibilities will require normalization of phagocytosis metrics
295 to progenitor abundance and/or assays that directly quantify engulfment kinetics per microglia.
296

297

298

299

300

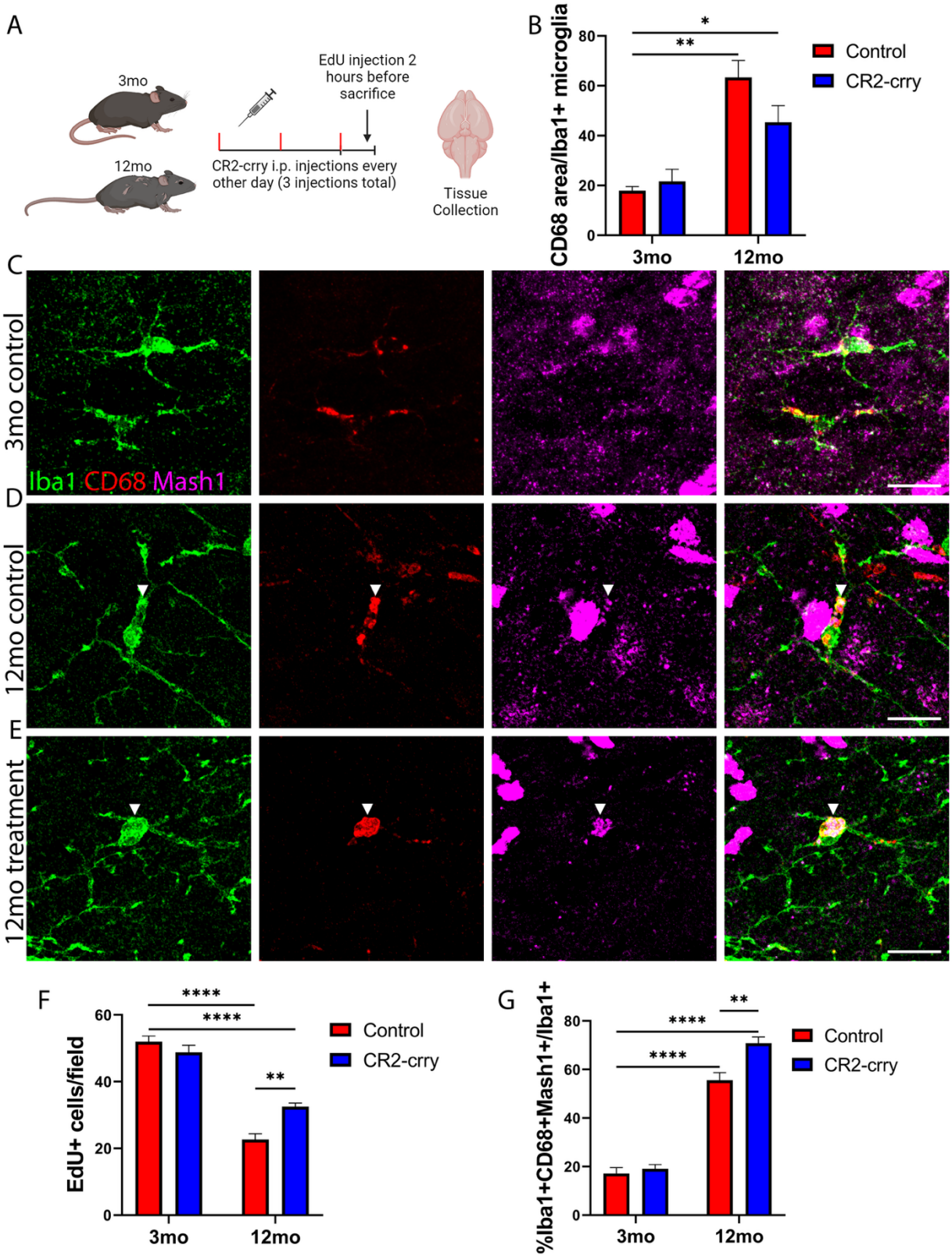
A
3mo
12mo
EdU injection 2 hours before sacrifice
CR2-crry i.p. injections every other day (3 injections total)
Tissue Collection
B
CD68 area/Iba1+ microglia
Control
CR2-crry
3mo
12mo
C
3mo control
Iba1 CD68 Mash1
D
12mo control
E
12mo treatment
F
EdU+ cells/field
G
%Iba1+CD68+Mash1+/Iba1+

301

302 **Figure 4. Complement inhibition partially rescues SVZ proliferation in aged mice yet further**
303 **increases SVZ microglia phagocytosis. (A)** Graphic representation of CR2-crry or saline
304 administration to young (3 month) or aged (12 month) mice. **(B)** Quantification of microglia
305 activation measured by CD68 area / number of microglia. Statistics: *n*=4 mice/group, ≥ 1,000
306 microglia quantified per mouse, p-values estimated using two-way ANOVA. **(C-E)** Confocal
307 projection images of young control, aged control, aged CR2-crry treated SVZ microglia stained
308 with Iba1 (green), microglia lysosomes stained with CD68 (red), and aNSC/TAC transcription
309 factor stained with Mash1 (magenta). Arrowheads in aged control and aged CR2-crry treated
310 indicate colocalization of Mash1+ signal within microglia lysosomes (Iba1+CD68+). Scale bar:
311 10µm. **(F)** Quantification of proliferating EdU-positive cells in the SVZ of young or aged control
312 or CR2-crry treated mice. Statistics: Same as in (B). **(G)** Quantification of Mash1 containing
313 microglia measured by Iba1+CD68+Mash1+ / number of Iba1+ cells from young or aged control
314 or CR2-crry treated mice. Statistics: Same as in (B). P-value legend: ns: no symbol; *: $p \leq 0.05$,
315 **: $p \leq 0.01$, ***: $p \leq 0.001$, ****: $p \leq 0.0001$.

316

317 Minocycline reduces SVZ microglial activation and partially restores
318 proliferation, but does not reduce progenitor-associated lysosomal signal

319 We previously reported that SVZ microglia exhibit elevated activation-associated features with
320 age, including increased CD68, consistent with a pro-inflammatory niche milieu (Solano et al.,
321 2016). We asked if broadly reducing the activation of aged SVZ microglia would result in
322 increased proliferation and/or reduced phagocytosis. To test whether broadly reducing microglial
323 activation in aged mice alters SVZ proliferative output and/or microglial phagocytic engagement
324 with SVZ progenitors, we treated young (3 month) and aged (12 month) mice with minocycline,
325 an antibiotic with well-described anti-inflammatory activity in the CNS, or saline for 14 days
326 (Elewa et al., 2006; Garrido-Mesa et al., 2013; Plane et al., 2010; Tikka et al., 2001; Yrjänheikki
327 et al., 1998). Mice received a 2-hour EdU pulse prior to sacrifice to label proliferating cells (Fig.
328 5A). SVZ wholemounts were collected and processed for immunohistochemistry as described
329 above.

330 In young mice, minocycline treatment did not significantly alter SVZ proliferation as indicated by
331 EdU+ cells, microglial CD68 area, or the fraction of microglia containing Mash1+ material within
332 CD68+ compartments (Figs. 5B-G). In contrast, in aged mice, minocycline significantly reduced
333 microglial CD68 area relative to saline-treated controls, consistent with attenuation of activation-
334 associated lysosomal features in the aged SVZ (Figs. 5B, D-E). Minocycline also increased SVZ
335 proliferation in aged mice relative to saline-treated aged controls, although proliferation remained
336 below levels observed in young mice (Fig. 5F).

337 As expected, fraction of microglia containing Mash1+ material within CD68+ compartments was
338 increased in aged saline-treated mice compared with young controls (Fig. 5C-D,G). Notably,
339 minocycline did not reduce this readout in aged mice; instead, it was further increased relative to
340 age-matched saline controls (Fig. 5E,G). These data indicate that broad anti-inflammatory
341 treatment can partially restore proliferative output in the aged SVZ while failing to decrease
342 microglial phagolysosomal association with Mash1+ progenitor material. As with the CR2-crry
343 treatment, a plausible explanation is that reducing inflammatory tone improves progenitor
344 production/maintenance, increasing Mash1+ substrate availability and thereby sustaining or
345 elevating the colocalization metric without necessarily increasing per-cell phagocytic propensity.
346 Alternatively, inflammatory suppression and progenitor engulfment may be regulated through
347 partially independent pathways in the aged SVZ.

348

349

350

351

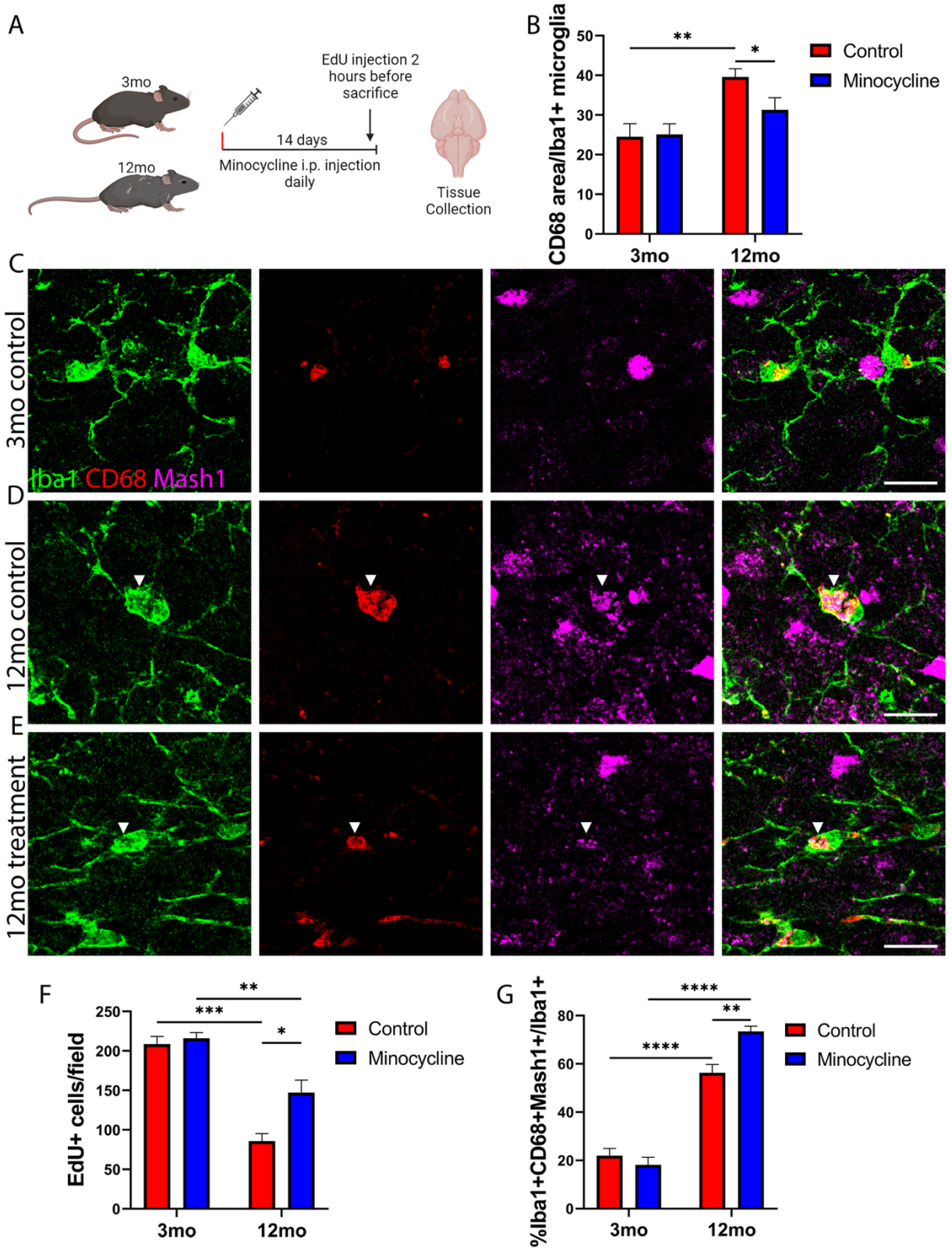
A
3mo
12mo
EdU injection 2 hours before sacrifice
14 days
Minocycline i.p. injection daily
Tissue Collection
B
CD68 area/Iba1+ microglia
Control
Minocycline
3mo
12mo
C
3mo control
Iba1 CD68 Mash1
D
12mo control
E
12mo treatment
F
EdU+ cells/field
G
%Iba1+CD68+Mash1+/Iba1+

352

Figure 5. Minocycline reduces SVZ microglial activation and partially restores proliferation, but does not reduce progenitor-associated lysosomal signal.

(A) Graphic representation of minocycline or saline administration to young (3 month) or aged (12 month) mice. **(B)** Quantification of microglia activation measured by CD68 area / number of microglia. Statistics: *n*=4 mice/group, ≥ 1,000 microglia quantified per mouse, p-values estimated using two-way ANOVA. **(C-E)** Confocal projection images of young control, aged control, aged minocycline treated SVZ microglia stained with Iba1 (green), microglia lysosomes stained with CD68 (red), and aNSC/TAC transcription factor stained with Mash1 (magenta). Arrowheads in aged control and aged minocycline treated indicate colocalization of Mash1+ signal within microglia lysosomes (Iba1+CD68+). Scale bar: 10µm. **(F)** Quantification of proliferating EdU-positive cells in the SVZ of young or aged control or minocycline treated mice. Statistics: Same as in (B). **(G)** Quantification of Mash1 containing microglia measured by Iba1+CD68+Mash1+ / number of Iba1+ cells from young or aged control or minocycline treated mice. Statistics: Same as in (B). P-value legend: ns: no symbol; *: $p \leq 0.05$, **: $p \leq 0.01$, ***: $p \leq 0.001$, ****: $p \leq 0.0001$.

Limitations

Several limitations should be considered when interpreting these findings. First, our *in vivo* phagocytosis readout relies on confocal colocalization of Mash1 signal within CD68+ compartments in Iba1+ microglia in SVZ wholemounts. While this pattern is consistent with phagolysosomal internalization, additional validation using phagosome markers or ultrastructural approaches will strengthen localization and interpretation. Second, the *in vitro* phagocytosis assay uses pHrodo-conjugated yeast/zymosan-like particles, which can engage receptors such as TLR2 and dectin-1. Consequently, the observed age- and region-dependent differences may reflect pathway-specific responsiveness rather than global phagocytic capacity. Testing alternative cargos (e.g., apoptotic bodies) and defined opsonization states will be necessary to assess generality. Third, although the CR2-Crry intervention is designed to inhibit C3 activation and deposition, we did not directly measure complement activation or target engagement within the SVZ following treatment. This limits causal inference about the extent and spatial specificity of complement

382 inhibition in the niche and makes it difficult to distinguish direct complement effects from
383 downstream or systemic consequences.

384 Additional caveats apply to generalizability and mechanistic resolution. Our work focuses on
385 discrete ages (3 and 12 months for most experiments), which captures a midlife transition but does
386 not resolve the temporal ordering of microglial activation, phagocytic engagement, and progenitor
387 decline across aging; denser longitudinal sampling would better establish sequence and potential
388 thresholds. Interventions (CR2-Crry and minocycline) are not microglia-specific and may act on
389 other niche cells or peripheral immune pathways, complicating attribution of effects to microglia
390 versus the broader SVZ environment. Moreover, increases in EdU+ counts provide a useful
391 proliferative readout but do not by themselves resolve whether the rescued proliferation reflects
392 altered cell-cycle dynamics, survival, lineage progression, or changes in the composition of
393 proliferating populations; additional phenotyping of EdU+ cells would sharpen interpretation.
394 Finally, the scRNA-seq reanalysis provides supportive mechanistic context, but transcriptomic
395 signatures cannot distinguish increased phagocytic "capacity" from compensatory programs or
396 assign directionality of cell–cell interactions; functional perturbations of candidate receptor–ligand
397 axes and direct measures of engulfment dynamics will be required to establish causality.

398

399 # Discussion

400 Adult SVZ NSCs generate new neurons that migrate to the OB and contribute to olfactory learning
401 and discrimination throughout life (Lledo & Valley, 2016). In addition, following brain injury SVZ
402 neural progenitors and neuroblast undergo a proliferative burst and then migrate to damaged areas
403 where they give rise to a limited number of neurons, astrocytes and oligodendrocytes and can also

404 secrete pro-reparative factors (Liang et al., 2019; Robin et al., 2006; Yamashita et al., 2006). The
405 blockade of this response results in larger legions and worsens behavioral deficits (Ohab et al.,
406 2006). Together, these observations support the SVZ as a candidate target for therapies aimed at
407 enhancing endogenous repair. However, SVZ neurogenesis declines drastically in aged rodents,
408 with the most-rapid reductions between midlife (9-12 months) and persists for the duration of
409 aging (Luo et al., 2006). This decline coincides with increasing risk of brain injury with age,
410 motivating a need to identify niche mechanisms that constrain SVZ stem/progenitor function. Our
411 data support a model in which aging is accompanied by increased microglial inflammatory and
412 phagocytic programs within the SVZ niche, together contributing to reduced stem/progenitor
413 output during aging.

414 During embryonic neurogenesis, SVZ-associated microglia display amoeboid morphology and can
415 regulate precursor pool size through phagocytosis of non-apoptotic neuroblasts (Cunningham et
416 al., 2013; Morrison et al., 2023). In the adult dentate gyrus, another neurogenic niche, microglia
417 phagocytose apoptotic newborn neurons as part of routine homeostasis, whereas apoptosis within
418 the adult SVZ is generally reported to be low (Luo et al., 2006). In the OB, where many SVZ-
419 derived neurons fail to integrate, phagocytic clearance is more prominent (Xavier et al., 2015). In
420 our study, we did not detect an age-associated increase in cleaved caspase-3 signal in the SVZ,
421 arguing against a simple model in which increased microglial lysosomal content in aging is driven
422 primarily by increased clearance of apoptotic SVZ progenitors. Instead, our *in vivo* colocalization
423 and *in vitro* phagocytosis assays are consistent with increased microglial phagocytic programs and
424 increased microglial association with Mash1+ progenitor-derived material in the aged niche,
425 although we emphasize that colocalization-based metrics are proxies and do not, on their own,
426 establish engulfment kinetics or target selectivity.

427 Reanalysis of published single-cell transcriptomes from young and old SVZ provided an
428 independent line of evidence consistent with increased inflammatory and phagocytosis-related
429 programs in aged microglia. In pseudobulk AGDGE and gene-set analyses, aged microglia
430 upregulated inflammatory signaling and lysosome/phagosome-associated genes, including
431 multiple receptors and effectors linked to phagocytic function (e.g., *Axl*, *Tlr2*, *Lgal3*, and *C3*), and
432 showed broader increases across several phagocytosis pathway components (e.g. Complement, FC
433 gamma, and Toll-like). In contrast, neural stem/progenitor populations exhibited comparatively
434 few significant age-related DE genes, motivating gene-set–level testing rather than threshold
435 overlaps. Those analyses suggested that astrocyte-qNSCs and neuroblasts increase
436 complement/opsonization-related expression (i.e. "eat-me" programs) while also increasing
437 expression of putative anti-phagocytic programs, including MHC class I/antigen presentation–
438 associated genes (i.e. "don't eat-me" programs). aNSCs-NPCs did not show the same pattern of
439 increased "don't eat-me" programs, which is consistent with, but does not prove, a model in which
440 aNSCs/ TACs may be relatively vulnerable to microglial phagocytic engagement in the aged niche.
441 Importantly, transcriptomic signatures cannot distinguish increased phagocytic capacity from
442 compensatory responses to altered substrate availability, nor can they assign directionality without
443 functional validation. The strength of the scRNA-seq analysis is therefore as mechanistic context
444 that complements the *in vivo* and *in vitro* assays.

445 Microglia are distributed throughout the brain, but exhibit region-dependent heterogeneity in
446 density, morphology, transcriptional state, and receptor expression shaped by local
447 microenvironments (Grabert et al., 2016; Tan et al., 2020). SVZ microglia are reported to be
448 phenotypically distinct from non-germinal regions, supporting the idea of niche specialization
449 (Goings et al., 2006; Marshall et al., 2014; Shigemoto-Mogami et al., 2014; Solano et al., 2016;

450 Xavier et al., 2015). Riberio Xavier et al. showed that SVZ microglia in young adults have distinct
451 morphology and receptor profiles, are required for neuroblast survival and migration, and display
452 comparatively low phagocytic activity in the young SVZ niche, potentially linked to reduced
453 expression of specific purinergic receptors (Xavier et al., 2015). Our *in vitro* assay is consistent
454 with this niche-specific baseline state. SVZ-derived microglia from young mice exhibited lower
455 phagocytic activity than microglia isolated from non-SVZ brain regions. With aging, we observe
456 a shift toward increased CD68+ lysosomal features and increased phagocytic readouts, consistent
457 with remodeling of this niche-specialized state.

458 To probe whether inflammatory signaling contributes causally to SVZ aging phenotypes, we used
459 two *in vivo* interventions: CR2-Crry, a targeted inhibitor of complement C3 activation and
460 deposition (Atkinson et al., 2005; Song et al., 2003) that crosses the blood brain barrier (Alawieh
461 et al., 2018) and minocycline, a broad anti-inflammatory agent often reported to reduce microglial
462 activation and confer neuroprotection (Ekdahl et al., 2003; Garrido-Mesa et al., 2013; Plane et al.,
463 2010; Tikka et al., 2001; Yrjänheikki et al., 1998). Both interventions partially rescued SVZ
464 proliferation in aged mice, supporting the conclusion that inflammatory signaling, including
465 complement-linked signaling, contributes to the age-associated reduction in proliferative output.
466 However, neither intervention reduced Mash1+ material within CD68+ compartments in aged
467 microglia; instead, both were associated with further increases. A parsimonious explanation is that
468 partial restoration of proliferation increases the production and/or persistence of aNCS/TACs,
469 thereby increasing substrate availability for microglial engagement and elevating a colocalization-
470 based metric even if per-cell phagocytic propensity is unchanged. An alternative explanation is
471 that inflammatory signaling and phagocytic engagement are governed by partially independent
472 regulatory pathways in the aged SVZ, such that reducing inflammation improves proliferation

473 without suppressing (and potentially indirectly enhancing) microglial phagocytic interactions.
474 Distinguishing these possibilities will require normalization of phagocytosis readouts to progenitor
475 abundance, direct quantification of engulfment dynamics, and mechanistic tests of candidate
476 receptor–ligand axes suggested by the transcriptomic analyses.

477 Finally, our transcriptomic observations raise a testable hypothesis about target susceptibility.
478 Aging may increase "eat-me" programs in multiple SVZ populations, while "don't eat-me"
479 programs may be relatively stronger in astrocyte-qNSCs and neuroblasts than in aNSCs and TACs.
480 If validated, this could help explain why increased microglial phagocytic programs in aging are
481 associated with progenitor loss while sparing other SVZ populations. Future work should directly
482 test whether differences in cell-surface inhibitory cues (e.g., *Cd200*, *Pecam1*, MHC class I–linked
483 programs) and corresponding microglial inhibitory receptors shape selective engagement of
484 progenitors in the aged niche, and whether manipulating these interactions can decouple restored
485 proliferation from progenitor loss, potentially paving the way for future therapeutics.

486

487 # Methods

488 ## Animals and Interventions

489 Male and female C57BL/6 mice were used in this study either bred at the UTHSA vivarium or
490 acquired from the National Institute of Aging. Young mice (3 months) and aged mice (12 months)
491 were housed in accordance with the University of Texas Health San Antonio Institutional Animal
492 Care and Use Committee and performed in accordance with institutional and federal guidelines
493 and allowed free access to water and standard rodent chow ad libitum.

494 Both male and female C57BL/6 mice received CR2-crry (10µg/1g mouse; Stephen Tomlinson
495 Lab, Medical University of South Carolina) or minocycline (50µg/1g mouse; Sigma-aldrich, Cat.
496 No. M9511) with respective saline controls via intraperitoneal injection. CR2-crry or saline was
497 administered every other day for a total of 3 doses. Minocycline or saline was administered daily
498 for 2 weeks.

499

500 **Immunohistochemistry**

501 The SVZ was isolated for wholemount (WM) tissue analysis; mice were anesthetized with
502 isoflurane, a cervical dislocation was performed, followed by brain extraction. Brains were placed
503 into cold HIB where they were halved and the septum and hippocampus were removed, and the
504 SVZ was microdissected from the surrounding brain tissue. The SVZ WM was then fixed in fresh
505 4% paraformaldehyde (PFA) for 30 minutes. SVZ WMs were permeabilized in 2% PBST and
506 blocked overnight at 4˚ C in 10% normal donkey serum (NDS). The SVZ WMs were then
507 incubated at 4°C for 4 days with primary antibody in blocking solution, followed by overnight
508 incubation at 4°C with secondary antibody made in blocking solution, and a 5-minute incubation
509 at room temperature (RT) with DAPI (1:1000; Invitrogen, Cat. No. D1306) then mounted on a
510 slide in ProLong Gold antifade reagent (Invitrogen, Cat. No. P36930). Primary antibodies that
511 were used include Iba1 (1:200; Wako, Cat. No. 019-19741 and 1:200; Novus, Cat. No. NB100-
512 1028), CD68 (1:250; BioRad, Cat. No. MCA1957), and Mash1 (1:5000; CosmoBioUSA, Cat. No.
513 SK-T01-003) Cleaved caspase 3 (1:200 Cell Signaling Cat. No D175 5A1E). Species-specific
514 secondary antibodies (Jackson ImmunoResearch) were used at a concentration of 1:500 in SVZ
515 WMs.

516

517 **Immunohistochemistry Quantification**

518 EdU was quantified in the SVZ by making a "Z Project" 2-dimensional image of the Z-stack in
519 ImageJ on 10 random fields of view and hand counting the number of EdU+ nuclei. The number
520 of microglia were quantified by hand counting Iba1+ cells, excluding cells whose cell body
521 touched the image boundary on Zen Microscopy Software (Zeiss). Total CD68 area was quantified
522 by making a "Z project" 2-dimensional image of the Z-stack, using the "Threshold" function, and
523 then the "Analyze particle" function to give total area in µm2 that was then averaged by total
524 number of microglia in each image. Total number of Iba1+ microglia were quantified similarly to
525 EdU+ cells described above. Mash1 colocalization within Iba1+ microglia were quantified by hand
526 counting in Zen Microscopy Software (Zeiss) by examining each Iba1+ microglia's lysosome
527 (CD68+) to determine if each Iba1+CD68+ microglia contained Mash1 colocalization. The
528 number of Mash1+CD68+Iba1+ microglia were then averaged to total number of Iba1+ microglia
529 in each image. There were no microglia that contained Mash1 that were not CD68+. SVZ WMs
530 were analyzed from 15µm thick Z-stacks (15 Z-stacks per WM). Confocal images were obtained
531 with a Zeiss LSM 710 confocal microscope at 40x objective.

532

533 **Single-cell RNA-sequencing quality control and filtering**

534 Quality control of downloaded single-cell RNA-Seq data (see Data Availability) was first
535 performed, which filtered cells where the number of genes or UMIs detected were greater or less
536 than 5 median absolute deviations (MADs) or percent mitochondria reads greater or less than 3

537 MADs, relative to all cells in the dataset. Genes were filtered if detected in less than 10 cells out
538 of all cells in the dataset. Cell identity labels were those assigned by the original analysis.

539

540 Single-cell RNA-sequencing differential expression and gene set enrichment 541 analysis

542 Pseudobulk samples were created by summing counts of each identified cell type for each
543 biological replicate. The DESeq2 package (Love et al., 2014) was then used to perform differential
544 expression analysis to compare old vs. young groups. Following this the ClusterProfiler package
545 (Yu et al., 2012) was then used to perform gene set enrichment analysis using the gene ontology
546 biological process database or custom annotations.

547

548 Microglia phagocytosis gene set analysis

549 Genes associated with known phagocytosis receptors and/or pathways active in microglia were
550 manually curated by searching the Molecular Signatures Database (MsigDB) and the literature
551 (i.e. Complement, Toll-like receptor, TAM receptor, Trem2 receptor, FC gamma, Pr2y6 receptor,
552 Scavenger receptor, Mannose receptor, LRP1 receptor, Galectin-3 adaptor protein, Microglia
553 Activation, Microglia Proliferation, Disease-Associated Microglia (DAM), and Microglia
554 Development). In addition, gene sets related to screens of phagocytosis regulators was obtained
555 from the literature (see Data Availability). These gene sets were then overlapped with the genes
556 that were found to be significantly differently expressed (adjusted p-value < 0.05) in the microglia
557 old vs. young comparison.

558

559 ## Neural stem cell gene set analysis

560 Genes associated with pathways known to be expressed in cells that are targeted for phagocytosis
561 were manually curated by searching the Molecular Signatures Database (MsigDB) and the
562 literature (i.e. Apoptosis, Opsonization, Antigen Processing and Presentation, "eat-me," "find-
563 me," and "don't eat me"). Because of the lack of genes which were significantly differentially
564 expressed in neural stem cells (i.e. Astrocytes/qNSCs, aNSCs/NPCs and Neuroblasts) in the old
565 vs. young comparison, the ClusterProfiler package was then used to perform gene set enrichment
566 analysis using the manually curated gene sets. The Log_2 fold change of genes within the gene sets
567 found to be significantly enriched in age-related genes expression of neural stem cells.

568

569 ## Microglia Isolation and Cell Culture

570 SVZ microglia were derived by mixed-glial expansion whereas whole brain microglia were
571 MACS-isolated. C57BL/6 mice were injected intraperitoneally with pentobarbital (25µL/mouse)
572 then perfused with cold 1x PBS. SVZ WMs or the remainder of the whole brain excluding the
573 SVZ and cerebellum, hereby referred to as whole brain (WB), were isolated following perfusion.
574 The tissues were minced and dissociated in 50U papain in DMEM/F12 at 37°C for 45 minutes and
575 manually triturated and spun 3x in DMEM. SVZ and WB homogenate were gently pressed through
576 a 70µm cell strainer to remove debris. For mixed glial culture, SVZ homogenate were then plated
577 in a T25 flask coated with poly-L-ornithine (PLO) in neural growth media (DMEM/F12, 5% fetal
578 bovine serum, 1x N2, 10ng/mL EGF, and 10ng/mL bFGF) until a confluent cell monolayer formed.
579 The culture was then fed microglia proliferation media (DMEM/F12, 10% fetal bovine serum, 1x

580 N2, and 20 ng/mL GM-CSF) until microglia could be seen atop the monolayer. Once microglia
581 were present, they were shaken off from the cell monolayer and the SVZ microglia could be plated
582 for further experimentation.

583 For microglia isolated by MACS, following the cell strainer step, WB homogenate was
584 resuspended in HIB and centrifugated at 400G with no brake in 22% Percoll (Sigma-aldrich, Cat.
585 No. P4937) solution to remove myelin from the samples. The WB homogenate was then
586 resuspended in 0.5% bovine serum albumin and incubated with 10µL CD11b Microbeads (cat#
587 130-093-636) per 107 cells. The homogenate was then placed in an LS column (MiltenyiBiotec,
588 Cat. No. 130-042-401) in a QuadroMACS™ separator (MiltenyiBiotec, Cat. No. 130-090-976) to
589 allow for MACS sorting of CD11b + microglia following manufacturer protocols
590 (MiltenyiBiotec). WB microglia were plated in a 6-well plate coated with PLO/laminin (10µg/mL;
591 Sigma-aldrich, Cat. No. L2020) at 250k cells/well in microglia expansion media (DMEM/F12,
592 100 µg/mL PenStrep, 5 µg/mL n-acetyl-L-cysteine, 5 µg/mL Insulin, 100 µg/mL apo-transferrin,
593 100 µg/mL sodium selenite, 1 µg/mL heparin sulfate, 10% fetal bovine serum, 1.5 µg/mL
594 cholesterol, 40 ng/mL M-CSF, 20 ng/mL GM-CSF, and 2 ng/mL TGF-β) adapted from [Bohlen et
595 al., 2017].

596

597 **Microglia *in vitro* Phagocytosis Assay**

598 The phagocytosis assay was performed using live cell imaging by Incucyte S3 (Essen BioScience)
599 for WB or SVZ microglia phagocytosis from 3- or 12-month mice. WB microglia were passaged
600 from a 6-well plate with Trypsin (Fisher, Cat. No. 25-200-072) following MACS isolation and
601 SVZ microglia were collected from mixed glial culture and microglia were plated in a 96 well

602 plate coated with PLO/laminin at 20k cells/well in microglia expansion media for 3 days. After 3
603 days, SVZ and WB microglia were moved to serum free media (DMEM/F12, 100 µg/mL PenStrep,
604 5 µg/mL n-acetyl-L-cysteine, 5 µg/mL Insulin, 100 µg/mL apo-transferrin, 100 µg/mL sodium
605 selenite, 1 µg/mL heparin sulfate, 1.5 µg/mL cholesterol, 40 ng/mL M-CSF, and 2 ng/mL TGF-β)
606 adapted from [Bohlen et al., 2017] for 1 week. All microglia were then incubated with 5 µg/mL
607 Isolectin IB4 Alexa Fluor™ 488 Conjugate (Invitrogen, Cat. No. I21411) for 60 minutes at 37°C.
608 SVZ or WB microglia of both ages were treated with Zymosan S. cerevisiae BioParticles™ (10
609 mg/mL; Invitrogen, Cat. No. Z2849) conjugated pHrodo™ Red SE (Molecular Probes™, Cat. No.
610 P36600) following manufacturer protocols (ThermoFisher) and adapted from [Haney et al., 2018;
611 Pluvinage et al., 2019], both Zymosan-pHrodo and Cytochalasin D (10 mM/µL Sigma-aldrich,
612 Cat. No. C8273) to inhibit phagocytosis, or isolectin only as a negative control. The microglia
613 were then incubated in the Incucyte S3 with fluorescent images captured every hour over the
614 course of 48 hours for live cell imaging of microglia phagocytosis. The images were analyzed in
615 the IncuCyte software (Essen BioScience) quantifying colocalization of the green fluorescence of
616 Isolectin IB4 labelled microglia and the red fluorescence of engulfed Zymosan-pHrodo within the
617 microglia lysosome demonstrating microglia phagocytosis. Total pHrodo area / number of
618 microglia was calculated for each well and condition yielding amount of in vitro phagocytosis
619 occurring at each time point.

620

621 **RNA Extraction and qPCR**

622 RNA was extracted from freshly isolated microglia following magnetic-activated cell sorting
623 (MACS) isolation, using a TRIzol-chloroform method (Rio et al., 2010) where cells were lysed in

624 TRIzol (Invitrogen, Cat. No. 15596018), aqueous layer separated with chloroform, RNA was
625 precipitated with isopropanol, washed in ethanol, dried, then resuspended in RNase-free water.
626 cDNA was synthesized using High Capacity cDNA Reverse Transcription Kit (Applied
627 Biosystems, Cat. No. 4368814). Quantitative polymerase chain reaction (qPCR) was performed
628 using a C1000 Touch Thermal Cycler (BioRad) with iTaq™ Universal SYBR® Green Supermix
629 (BioRad, Cat. No. 1725121). Reactions were performed in doublet with glyceraldehyde-3-
630 phosphate dehydrogenase (GAPDH) used as an endogenous control. Negative control reactions
631 were performed using the same conditions without cDNA. Quantification was analyzed using the
632 ΔΔCt method as described [Livak and Schmittgen, 2001]. Primers were used for the following
633 transcripts: C1QA, P2Y12, TREM2, LPAR, C3, CR1, ITGAM, ITGAX, GAPDH.

Primers	Forward	Reverse
C1QA	AAAGGCAATCCAGGCAATATCA	TGGTTCTGGTATGGACTCTCC
C3	CCAGCTCCCCATTAGCTCTG	GCACTTGCCTCTTTAGGAAGTC
TREM2	CTGGAACCGTCACCATCACTC	CGAAACTCGATGACTCCTCGG
LPAR	AGCCATGAACGAACAACAGTG	CATGATGAACACGCAAACAGTG
CR1	ATGGAGGTCTCTTCTCGGAGT	GGCCGAAGGCTACAAGGAG
ITGAM	GGGAGGACAAAAACTGCCTCA	ACAACTAGGATCTTCGCAGCAT
ITGAX	CTGGATAGCCTTTCTTCTGCTG	GCACACTGTGTCCGAACTCA
GAPDH	AGGTCGGTGTGAACGGATTTG	TGTAGACCATGTAGTTGAGGTCA

634

635 **EdU Labeling and Staining**

636 Mice were injected intraperitoneally (50µg EdU/1g mouse) 2 hours before sacrifice. Their brains
637 were removed and SVZ was isolated and fixed for 30 minutes in 4% PFA. EdU staining was
638 performed following manufacturer protocols (Fisher, Click-it EdU Imaging Kit, Cat. No. C10337).

639

640 **Data Analysis**

641 Student's t-tests and two-way ANOVA were used to analyze the data on GraphPad Prism 8
642 Software. All data are expressed as mean ± standard error of the mean.

643

644 **Data Availability**

645 Normalized single-cell RNA-sequencing data and cell type annotations of the SVZ from young (3
646 months old) and old (28–29 months old) male mice (n = 3) was downloaded from Supplementary
647 Table 2 of the Dulken et al., 2019 study. Results of screen for phagocytosis regulator genes were
648 downloaded from Supplementary Table 5 of the Haney et al., 2019 study and Supplementary Table
649 2 of the Pluvinage et al., 2019 study. Marker genes of major cell types in the SVZ of young (2-4
650 months old) male and female mice were downloaded from Table S1 of the Zywitza et al., 2018
651 study.

652

653

654

Code Availability

Code to reproduce bioinformatics analyses is available at the following repository: https://github.com/cutleraging/nsc-aging

References

Ahlenius, H., Laboratory of Neural Stem Cell Biology, Lund Stem Cell Center, S.-L., Sweden, Visan, V., Laboratory of Neurogenesis and Cell Therapy, a., Lund Stem Cell Center, S.-L., Sweden, Kokaia, M., Experimental Epilepsy Group, S. o. R. N., Wallenberg Neuroscience Center, University Hospital, SE-221 84 Lund, Sweden, and, Lindvall, O., Laboratory of Neurogenesis and Cell Therapy, a., Lund Stem Cell Center, S.-L., Sweden, Kokaia, Z., Laboratory of Neural Stem Cell Biology, & Lund Stem Cell Center, S.-L., Sweden. (2025). Neural Stem and Progenitor Cells Retain Their Potential for Proliferation and Differentiation into Functional Neurons Despite Lower Number in Aged Brain. *The Journal of Neuroscience*, *29*(14), 4408. https://doi.org/10.1523/JNEUROSCI.6003-08.2009

Alawieh, A., J, Z., & W, F. (2018). Factors affecting post-stroke motor recovery: Implications on neurotherapy after brain injury. *Behavioural brain research*, *340*. https://doi.org/10.1016/j.bbr.2016.08.029

Alvarez-Buylla, A., & García-Verdugo. (2002). Neurogenesis in Adult Subventricular Zone. *The Journal of Neuroscience*, *22*(3), 629. https://doi.org/10.1523/JNEUROSCI.22-03-00629.2002

Atkinson, C., Song, H., Lu, B., Qiao, F., Burns, T. A., Holers, V. M., Tsokos, G. C., & Tomlinson, S. (2005). Targeted complement inhibition by C3d recognition ameliorates tissue injury without apparent increase in susceptibility to infection. *Journal of Clinical Investigation*, *115*(9), 2444. https://doi.org/10.1172/JCI25208

Cunningham, C. L., Martínez-Cerdeño, V., & Noctor, S. C. (2013). Microglia regulate the number of neural precursor cells in the developing cerebral cortex. *J Neurosci*, *33*(10), 4216-4233. https://doi.org/10.1523/JNEUROSCI.3441-12.2013

Cutler, R. R., & Kokovay, E. (2020). Rejuvenating subventricular zone neurogenesis in the aging brain. *Curr Opin Pharmacol*, *50*, 1-8. https://doi.org/10.1016/j.coph.2019.10.005

Deczkowska, A., Keren-Shaul, H., Weiner, A., Colonna, M., Schwartz, M., & Amit, I. (2018). Disease-Associated Microglia: A Universal Immune Sensor of Neurodegeneration. In A. W. Hadas Keren-Shaul 1 2 5, Marco Colonna 3, Michal Schwartz 4, Ido Amit 1 (Ed.). Cell.

Doetsch, F., Caillé, I., Lim, D. A., García-Verdugo, J. M., & Alvarez-Buylla, A. (1999). Subventricular zone astrocytes are neural stem cells in the adult mammalian brain. *Cell*, *97*(6), 703-716. https://doi.org/10.1016/s0092-8674(00)80783-7

692 Dulken, B. W., Buckley, M. T., Navarro Negredo, P., Saligrama, N., Cayrol, R., Leeman, D. S.,
693 George, B. M., Boutet, S. C., Hebestreit, K., Pluvinage, J. V., Wyss-Coray, T., Weissman,
694 I. L., Vogel, H., Davis, M. M., & Brunet, A. (2019). Single-cell analysis reveals T cell
695 infiltration in old neurogenic niches. *Nature*, *571*(7764), 205-210.
696 https://doi.org/10.1038/s41586-019-1362-5
697 Ekdahl, C., JH, C., S, B., Z, K., & O, L. (2003). Inflammation is detrimental for neurogenesis in
698 adult brain. *Proceedings of the National Academy of Sciences of the United States of*
699 *America*, *100*(23). https://doi.org/10.1073/pnas.2234031100
700 Elewa, H. F., Hilali, H., Hess, D. C., Machado, L. S., & Fagan, S. C. (2006). Minocycline for
701 Acute Neuroprotection. *Pharmacotherapy*, *26*(4), 515.
702 https://doi.org/10.1592/phco.26.4.515
703 Enwere, E., Shingo, T., Gregg, C., Fujikawa, H., Ohta, S., & Weiss, S. (2004). Aging Results in
704 Reduced Epidermal Growth Factor Receptor Signaling, Diminished Olfactory
705 Neurogenesis, and Deficits in Fine Olfactory Discrimination. *The Journal of*
706 *Neuroscience*, *24*(38), 8354. https://doi.org/10.1523/JNEUROSCI.2751-04.2004
707 Garrido-Mesa, N., Zarzuelo, A., & Gálvez, J. (2013). Minocycline: far beyond an antibiotic.
708 *British Journal of Pharmacology*, *169*(2), 337. https://doi.org/10.1111/bph.12139
709 Ginhoux, M, G., M, L., S, N., P, S., S, G., MF, M., SJ, C., LG, N., ER, S., IM, S., & M, M.
710 (2010). Fate mapping analysis reveals that adult microglia derive from primitive
711 macrophages. *Science (New York, N.Y.)*, *330*(6005).
712 https://doi.org/10.1126/science.1194637
713 Goings, DA, K., & FG, S. (2006). Differential activation of microglia in neurogenic versus non-
714 neurogenic regions of the forebrain. *Glia*, *54*(4). https://doi.org/10.1002/glia.20381
715 Grabert, K., T, M., MH, K., S, C., JK, B., MP, S., TC, F., KM, S., & BW, M. (2016). Microglial
716 brain region-dependent diversity and selective regional sensitivities to aging. *Nature*
717 *neuroscience*, *19*(3). https://doi.org/10.1038/nn.4222
718 Haney, M. S., Bohlen, C. J., Morgens, D. W., Ousey, J. A., Barkal, A. A., Tsui, C. K., Ego, B. K.,
719 Levin, R., Kamber, R. A., Collins, H., Tucker, A., Li, A., Vorselen, D., Labitigan, L.,
720 Crane, E., Boyle, E., Jiang, L., Chan, J., Rincón, E.,…Bassik, M. C. (2018). Identification
721 of phagocytosis regulators using magnetic genome-wide CRISPR screens. *Nat Genet*,
722 *50*(12), 1716-1727. https://doi.org/10.1038/s41588-018-0254-1
723 Hu, B., Fujian Provincial Key Laboratory of Neurodegenerative Disease and Aging Research, S.
724 o. M., Institute of Neuroscience, Xiamen University, Xiamen, China, Duan, S., Fujian
725 Provincial Key Laboratory of Neurodegenerative Disease and Aging Research, S. o. M.,
726 Institute of Neuroscience, Xiamen University, Xiamen, China, Wang, Z., Fujian
727 Provincial Key Laboratory of Neurodegenerative Disease and Aging Research, S. o. M.,
728 Institute of Neuroscience, Xiamen University, Xiamen, China, Li, X., Fujian Provincial
729 Key Laboratory of Neurodegenerative Disease and Aging Research, S. o. M., Institute of
730 Neuroscience, Xiamen University, Xiamen, China, Zhou, Y., Fujian Provincial Key
731 Laboratory of Neurodegenerative Disease and Aging Research, S. o. M., Institute of
732 Neuroscience, Xiamen University, Xiamen, China, Zhang, X., Fujian Provincial Key
733 Laboratory of Neurodegenerative Disease and Aging Research, S. o. M., Institute of
734 Neuroscience, Xiamen University, Xiamen, China, Zhang, Y.-W., Fujian Provincial Key
735 Laboratory of Neurodegenerative Disease and Aging Research, S. o. M., Institute of
736 Neuroscience, Xiamen University, Xiamen, China, Xu, H., Fujian Provincial Key
737 Laboratory of Neurodegenerative Disease and Aging Research, S. o. M., Institute of

Neuroscience, Xiamen University, Xiamen, China, Zheng, H., Fujian Provincial Key Laboratory of Neurodegenerative Disease and Aging Research, S. o. M., Institute of Neuroscience, Xiamen University, Xiamen, China, & Basic Medical Sciences, S. o. M., Xiamen University, Xiamen, China. (2024). Insights Into the Role of CSF1R in the Central Nervous System and Neurological Disorders. *Frontiers in Aging Neuroscience*, *13*, 789834. https://doi.org/10.3389/fnagi.2021.789834

Izgi, H., Han, D., Isildak, U., Huang, S., Kocabiyik, E., Khaitovich, P., Somel, M., & Dönertaş, H. M. (2022). Inter-tissue convergence of gene expression during ageing suggests age-related loss of tissue and cellular identity. *Elife*, *11*. https://doi.org/10.7554/eLife.68048

Kalamakis, G., Brüne, D., Ravichandran, S., Bolz, J., Fan, W., Ziebell, F., Stiehl, T., Catalá-Martinez, F., Kupke, J., Zhao, S., Llorens-Bobadilla, E., Bauer, K., Limpert, S., Berger, B., Christen, U., Schmezer, P., Mallm, J. P., Berninger, B., Anders, S.,…Martin-Villalba, A. (2019). Quiescence Modulates Stem Cell Maintenance and Regenerative Capacity in the Aging Brain. *Cell*, *176*(6), 1407-1419.e1414. https://doi.org/10.1016/j.cell.2019.01.040

Kapellos, T. S., Taylor, L., Lee, H., Cowley, S. A., James, W. S., Iqbal, A. J., & Greaves, D. R. (2016). A novel real time imaging platform to quantify macrophage phagocytosis. *Biochemical Pharmacology*, *116*, 107. https://doi.org/10.1016/j.bcp.2016.07.011

Khalaji, A., Yancheshmeh, F. B., Farham, F., Khorram, A., Sheshbolouki, S., Zokaei, M., Vatankhah, F., & Soleymani-Goloujeh, M. (2023). Don't eat me/eat me signals as a novel strategy in cancer immunotherapy. *Heliyon*, *9*(10), e20507. https://doi.org/10.1016/j.heliyon.2023.e20507

Kim, E. J., Ables, J. L., Dickel, L. K., Eisch, A. J., & Johnson, J. E. (2011). Ascl1 (Mash1) Defines Cells with Long-Term Neurogenic Potential in Subgranular and Subventricular Zones in Adult Mouse Brain. *PLoS One*, *6*(3). https://doi.org/10.1371/journal.pone.0018472

Li, W. (2012). Eat-me signals: keys to molecular phagocyte biology and "appetite" control. *J Cell Physiol*, *227*(4), 1291-1297. https://doi.org/10.1002/jcp.22815

Liang, H., H, Z., A, G., M, M., S, T., S, T., M, R., J, R., & ST, C. (2019). Region-specific and activity-dependent regulation of SVZ neurogenesis and recovery after stroke. *Proceedings of the National Academy of Sciences of the United States of America*, *116*(27). https://doi.org/10.1073/pnas.1811825116

Liberzon, A., Broad Institute of MIT and Harvard, M. S. C., MA 02142, USA, Birger, C., Broad Institute of MIT and Harvard, M. S. C., MA 02142, USA, Thorvaldsdóttir, H., Broad Institute of MIT and Harvard, M. S. C., MA 02142, USA, Ghandi, M., Broad Institute of MIT and Harvard, M. S. C., MA 02142, USA, Mesirov, J. P., Broad Institute of MIT and Harvard, M. S. C., MA 02142, USA, Department of Medicine, U. S. D., La Jolla, CA 92093, USA, Moores Cancer Center, U. S. D., La Jolla, CA 92093, USA, Tamayo, P., Broad Institute of MIT and Harvard, M. S. C., MA 02142, USA, Department of Medicine, U. S. D., La Jolla, CA 92093, USA, & Moores Cancer Center, U. S. D., La Jolla, CA 92093, USA. (2024). The Molecular Signatures Database (MSigDB) hallmark gene set collection. *Cell systems*, *1*(6), 417. https://doi.org/10.1016/j.cels.2015.12.004

Lim, D. A., & Alvarez-Buylla, A. (2016). The Adult Ventricular–Subventricular Zone (V-SVZ) and Olfactory Bulb (OB) Neurogenesis. *Cold Spring Harbor Perspectives in Biology*, *8*(5). https://doi.org/10.1101/cshperspect.a018820

783 Lledo, P., & Valley, M. (2016). Adult Olfactory Bulb Neurogenesis. *Cold Spring Harbor*
784 *Perspectives in Biology*, *8*(8). https://doi.org/10.1101/cshperspect.a018945
785 Love, M. I., Huber, W., & Anders, S. (2014). Moderated estimation of fold change and dispersion
786 for RNA-seq data with DESeq2. *Genome Biol*, *15*(12), 550.
787 https://doi.org/10.1186/s13059-014-0550-8
788 Luo, J., SB, D., JB, L., RQ, N., & JC, C. (2006). The aging neurogenic subventricular zone.
789 *Aging cell*, *5*(2). https://doi.org/10.1111/j.1474-9726.2006.00197.x
790 Marshall, G. P., Deleyrolle, L. P., Reynolds, B. A., Steindler, D. A., & Laywell, E. D. (2014).
791 Microglia from neurogenic and non-neurogenic regions display differential proliferative
792 potential and neuroblast support. *Frontiers in Cellular Neuroscience*, *8*, 180.
793 https://doi.org/10.3389/fncel.2014.00180
794 Maslov, A. Y., Barone, T. A., Plunkett, R. J., & Pruitt, S. C. (2004). Neural Stem Cell Detection,
795 Characterization, and Age-Related Changes in the Subventricular Zone of Mice. *The*
796 *Journal of Neuroscience*, *24*(7), 1726. https://doi.org/10.1523/JNEUROSCI.4608-
797 03.2004
798 Morrison, V., MG, H., JB, T., AA, B., PJ, K., KA, K., HM, L., G, N.-J., AJ, T., KA, M.-Z., LJ,
799 M., GJ, B., RA, I., & BD, C. (2023). Jedi-1/MEGF12-mediated phagocytosis controls the
800 pro-neurogenic properties of microglia in the ventricular-subventricular zone. *bioRxiv :*
801 *the preprint server for biology*. https://doi.org/10.1101/2023.03.03.531012
802 Nath, S., Martínez Santamaría, J. C., Chu, Y.-H., Choi, J. S., Conforti, P., Lin, J.-D., Sankowski,
803 R., Amann, L., Galanis, C., Wu, K., Deshpande, S. S., Vlachos, A., Prinz, M., Lee, J. K.,
804 & Schachtrup, C. (2024). Interaction between subventricular zone microglia and neural
805 stem cells impacts the neurogenic response in a mouse model of cortical ischemic stroke.
806 *Nature communications*, *15*(1), 9095. https://doi.org/10.1038/s41467-024-53217-1
807 Ohab, J., S, F., A, B., & ST, C. (2006). A neurovascular niche for neurogenesis after stroke. *The*
808 *Journal of neuroscience : the official journal of the Society for Neuroscience*, *26*(50).
809 https://doi.org/10.1523/JNEUROSCI.4323-06.2006
810 Plane, D. J. M., Shen, D. Y., Pleasure, D. D. E., & Deng, D. W. (2010). Prospects for
811 Minocycline Neuroprotection. *Archives of neurology*, *67*(12), 1442.
812 https://doi.org/10.1001/archneurol.2010.191
813 Pluvinage, J. V., Haney, M. S., Smith, B. A. H., Sun, J., Iram, T., Bonanno, L., Li, L., Lee, D. P.,
814 Morgens, D. W., Yang, A. C., Shuken, S. R., Gate, D., Scott, M., Khatri, P., Luo, J.,
815 Bertozzi, C. R., Bassik, M. C., & Wyss-Coray, T. (2019). CD22 blockade restores
816 homeostatic microglial phagocytosis in ageing brains. *Nature*, *568*(7751), 187-192.
817 https://doi.org/10.1038/s41586-019-1088-4
818 Robin, A., ZG, Z., L, W., RL, Z., M, K., L, Z., Y, W., C, Z., & M, C. (2006). Stromal cell-derived
819 factor 1alpha mediates neural progenitor cell motility after focal cerebral ischemia.
820 *Journal of cerebral blood flow and metabolism : official journal of the International*
821 *Society of Cerebral Blood Flow and Metabolism*, *26*(1).
822 https://doi.org/10.1038/sj.jcbfm.9600172
823 Shigemoto-Mogami, Y., Hoshikawa, K., Goldman, J. E., Sekino, Y., & Sato, K. (2014).
824 Microglia Enhance Neurogenesis and Oligodendrogenesis in the Early Postnatal
825 Subventricular Zone. *The Journal of Neuroscience*, *34*(6), 2231.
826 https://doi.org/10.1523/JNEUROSCI.1619-13.2014
827 Solano, F., S, M., DM, A., R, R., A, D., A, C., J, O. C., & E, K. (2016). Neurogenic Niche
828 Microglia Undergo Positional Remodeling and Progressive Activation Contributing to

Age-Associated Reductions in Neurogenesis. *Stem cells and development*, *25*(7). https://doi.org/10.1089/scd.2015.0319

Song, H., He, C., Knaak, C., Guthridge, J. M., Holers, V. M., & Tomlinson, S. (2003). Complement receptor 2–mediated targeting of complement inhibitors to sites of complement activation. *Journal of Clinical Investigation*, *111*(12), 1875. https://doi.org/10.1172/JCI17348

Tan, Y., Y, Y., & L, T. (2020). Microglial regional heterogeneity and its role in the brain. *Molecular psychiatry*, *25*(2). https://doi.org/10.1038/s41380-019-0609-8

Tikka, T., Fiebich, B. L., Goldsteins, G., Keinänen, R., & Koistinaho, J. (2001). Minocycline, a Tetracycline Derivative, Is Neuroprotective against Excitotoxicity by Inhibiting Activation and Proliferation of Microglia. *The Journal of Neuroscience*, *21*(8), 2580. https://doi.org/10.1523/JNEUROSCI.21-08-02580.2001

Xavier, A. R., BT, K., SA, G., JR, L. d. M., & M, N. (2015). A Distinct Population of Microglia Supports Adult Neurogenesis in the Subventricular Zone. *The Journal of neuroscience : the official journal of the Society for Neuroscience*, *35*(34). https://doi.org/10.1523/JNEUROSCI.1217-15.2015

Yamashita, T., M, N., P, H. A., JM, G.-V., T, S., M, S., K, A., T, K., Y, H., T, K., N, A., K, A., H, O., & K, S. (2006). Subventricular zone-derived neuroblasts migrate and differentiate into mature neurons in the post-stroke adult striatum. *The Journal of neuroscience : the official journal of the Society for Neuroscience*, *26*(24). https://doi.org/10.1523/JNEUROSCI.0149-06.2006

Yen, J.-H. J., & Yu, I.-C. I. (2024). The role of ApoE-mediated microglial lipid metabolism in brain aging and disease. *Immunometabolism (Cobham (Surrey, England)*, *5*(1). https://doi.org/10.1097/IN9.0000000000000018

Yrjänheikki, J., Keinänen, R., Pellikka, M., Hökfelt, T., & Koistinaho, J. (1998). Tetracyclines inhibit microglial activation and are neuroprotective in global brain ischemia. *Proceedings of the National Academy of Sciences of the United States of America*, *95*(26), 15769. https://doi.org/10.1073/pnas.95.26.15769

Yu, G., LG, W., Y, H., & QY, H. (2012). clusterProfiler: an R package for comparing biological themes among gene clusters. *Omics : a journal of integrative biology*, *16*(5). https://doi.org/10.1089/omi.2011.0118